JOURNAL OF SOLID STATE CHEMISTRY **135,** 78–85 (1998)
ARTICLE NO. SC977596

Structural Characterization of Nanocrystalline SnO_2 by X-Ray and Raman Spectroscopy

L. Abello,* B. Bochu,† A. Gaskov,‡ S. Koudryavtseva,‡ G. Lucazeau,*,[1] and M. Roumyantseva‡

*LEPMI, ENSEEG, 38130 Grenoble, France; †LMGP, ENSPG, 38130 Grenoble, France; and ‡Chemistry Department, Moscow State University, 11899 Russia

Received April 11, 1997; in revised form August 11, 1997; accepted August 19, 1997

Tin dioxide nanocrystalline powders were prepared by precipitation of α-stannic acid followed by various thermal and chemical treatments. An original preparation via a colloidal solution step led to particles having a particular two-dimensional microstructure. The size of the crystallites was found to increase from 2 nm for as-prepared samples to 30 nm for samples annealed for 3.5 hr at 920°C. The compounds were characterized by X-ray diffraction, scanning electron microscopy (SEM), and infrared and micro-Raman spectroscopy. As reported in the literature, the Raman spectral signature was found to change drastically with the size of the particles. A new spectral feature centered at about 500 cm^{-1} was found for compounds prepared via the colloidal step and having typical sizes smaller than 4.5 nm. The powder Raman spectra are interpreted in terms of volume modes and surface modes. Their frequency evolution with crystallite size is discussed in terms of tensile surface stresses. © 1998 Academic Press

INTRODUCTION

Polycrystalline SnO_2, used as transparent electrodes (1) and as a solid-state gas sensor (2), is attracting much interest with regard to relationships between its electrical properties and crystallite size.

Low-dimensional systems such as nanocrystallites, thin films, two-dimensional heterostructures, clusters, and surface layers demonstrate a variety of chemical, physical, and functional properties different from those of the bulk materials. The influence of crystallite size on material properties is especially remarkable for polycrystalline thin films and ceramic samples.

The IR and Raman techniques are able to deliver structural information on amorphous and poorly crystallized samples. Usually the disorder induces spectral changes which are discussed in the frame of bulk crystal spectra and on their vibrational density of states. Tin oxide gives rise to well-defined Raman spectra (3), and the dynamics of rutile-like compounds has been extensively studied (3–5). However, for nanometric crystallites the surface atoms represent a nonnegligible fraction of atoms and give rise to specific spectral changes. Since the early IR study of Luxon and Summitt (6) on 0.5-μm spherical particles of SnO_2, it has been amply demonstrated (7) that the position, intensity, and width of the IR bands of microcrystalline SnO_2 particles are strongly affected by the shape and the state of aggregation. In the same way, several Raman studies report on the relationship between the size and the spectral changes in nanocrystallites of SnO_2 (8–10).

The aim of the present work is to characterize by X-ray diffraction and Raman spectroscopy the crystalline structural changes and the real microstructure of various nanocrystalline SnO_2 samples as powders and as layers prepared following different routes. We would also like to obtain a catalog of corresponding Raman spectra able to represent the size and shape of the crystallites and their state of aggregation.

These preliminary results are to be used to monitor the spectral changes that can take place when the samples are treated in an H_2S atmosphere.

MODELS FOR INTERPRETATION OF SIZE AND SHAPE EFFECTS ON SPECTRAL CHANGES

Infinite Crystal

Tin dioxide crystallizes in the D_{4h}^{14} space group and its structure is of the rutile type. The unit cell contains two formulas; the cations are located on D_{2h} sites and the oxygens are on C_{2v} sites. Three of the four expected Raman-active modes—A_{1g} (638 cm^{-1}), E_g (476 cm^{-1}), and B_{2g} (782 cm^{-1})—are observed (3). The B_{1g} mode corresponds to a librational motion of octahedra (11) and is reported at about 122 cm^{-1} (4). The dispersion relations for phonons propagating along various directions have been reported in refs 3 and 5.

Nanocrystallites

In ionic crystals the frequencies of the IR modes are strongly dependent on long-range Coulombic and dipolar

[1]To whom correspondence should be addressed.

0022-4596/98 $25.00

interactions and are thus related to dielectric constants. All models (7, 11) take into account the size and shape of the active particle embedded in a given medium. The high-frequency E_u and A_{2u} modes in nanocrystallites of SnO_2 undergo a frequency shift of about 100 cm^{-1} when the shape evolves from elongated (prolate) to flat (oblate) particles. The shape changes were reported as a function of the annealing time (7). Finally, the filling factor, defined as the fraction of total volume occupied by particles, is a parameter included in the models used for interpreting the IR spectral changes. Although this work is not concerned with IR measurements, one must be prepared to consider that ungerade modes can become observable in Raman as a consequence of disorder.

For Raman-active modes, three approaches can be considered:

(i) One consists in separating surface modes from bulk modes. For instance, the p_1 band in Fig. 2 of ref 9 at 576 cm^{-1} which grows when the size of the SnO_2 particles decreases is attributed to surface modes (9). In this respect a perfect linear correlation between the relative intensity of the surface modes centered on 572 cm^{-1} and the number of surface atoms can be deduced from Figs. 2 and 3 of ref 8. These results will be discussed further.

(ii) For interpreting the frequency shifts and the broadening of bands when crystallite size decreases, it is possible to consider that the normal modes of a finite particle are those of the infinite crystal which present nodes at the surface of the particle. This model implies that there are no more q vector selection rules. Thus using the phonon dispersion curves of refs. (3) and (5), one may speculate that the modes corresponding to $\Gamma_1 + (A_{1g})$ and belonging to the Λ_1 direction are expected to be between the 640 cm^{-1} (A_{1g}) center-zone mode and the 550-cm^{-1} Z_1 corner-zone mode. In this model the width of the bands would reveal a distribution of sizes. In microcrystalline silicon the localization of phonons in a spherical crystallite of diameter L has been achieved via a Gaussian modulation ($a \exp(-br^2/L^2)$) of the wave function of the infinite crystal (13, 14).

(iii) Finally, we would like to mention that the optical and acoustical modes of nanocrystals such as CdSe (15, 16) have been interpreted as a result of the interaction of light with vibrational eigenmodes of spheres. We have not tried to work in this direction.

EXPERIMENTAL

Samples

SnO_2 powders with different grain sizes and microstructures were fabricated by two methods starting from α-stannic acid prepared by reaction of $SnCl_4 \cdot 5H_2O$ with ammonia. The sequence of operation steps is given in Fig. 1.

Samples A and B were prepared by forming $Na_2Sn(OH)_6$, and after proton exchange for sodium, a colloidal solution was obtained and then dehydrated.

Samples C, D, and E were prepared directly from the dehydration of α-stannic acid. The different heat treatments are summarized in Fig. 2, where the annealing time is plotted on the x-axis and the average size of the particles deduced from X-ray diffraction (XRD) analysis (see next section) is plotted on the y-axis. The different samples are identified in this figure by the letters A to E.

Natural polycrystalline cassiterite was also used for obtaining reference spectra.

XRD and SEM Characterization

X-ray diffraction patterns were obtained using a Siemens diffractometer with monochromatic Cu$K\alpha$ radiation. The SnO_2 average sizes, which depend on the synthesis conditions, were calculated from the X-ray diffraction diagrams using the Debye–Scherrer formula: $d = K\lambda/\beta \cos\theta$, where d is the dimension of the particles, $K = 0.9$, $\lambda(\text{Cu}K\alpha) =$ 1.54051 Å, and β is the breadth of the diffraction lines. The standard value of the X-ray reflection widths measured in the 2θ range from 10° to 80° with polycrystalline LaB_6 is 0.085.

Natural polycrystalline cassiterite was used for reference spectra. Scanning electron microscopy (Philips XL30) was used to study the morphology of the microstructure.

Raman and Infrared Spectroscopy

Raman spectra were obtained using a DILOR XY multichannel spectrometer. The 514.5-nm exciting line of an argon laser was focused on the samples through the $G = 50$ and 100 objectives of a microscope such that the diameter of the analyzed area was about 1 μm. The laser beam power on the sample was limited to 3 mW to prevent heating of the samples. The average spectral width was ca. 3.5 cm^{-1}. The samples were investigated at 300 K under a dry air atmosphere.

Infrared spectra were obtained on a BioRad FTS 135 spectrometer. The powders were dispersed in CsI (1.5 mg/150 mg) and were studied at 300 K. The spectral resolution was 4 cm^{-1}.

RESULTS

XRD and SEM Analysis

All the samples exhibit the cassiterite SnO_2 structure. The line width depends on the synthesis process and on the annealing temperature. Figure 3 shows the XRD of the different samples obtained under the various conditions.

The diffraction lines represented in Fig. 3 are the following (their *hkl* indices are given in parentheses): 27.716 (110), 34.004 (101), 38.087 (200), 39.117 (111), 51.898 (211), 54.894 (220), 57.952 (002), 62.010 (310), 64.860 (112), and 66.092 (301). The differences between diagrams C, D, and E on the

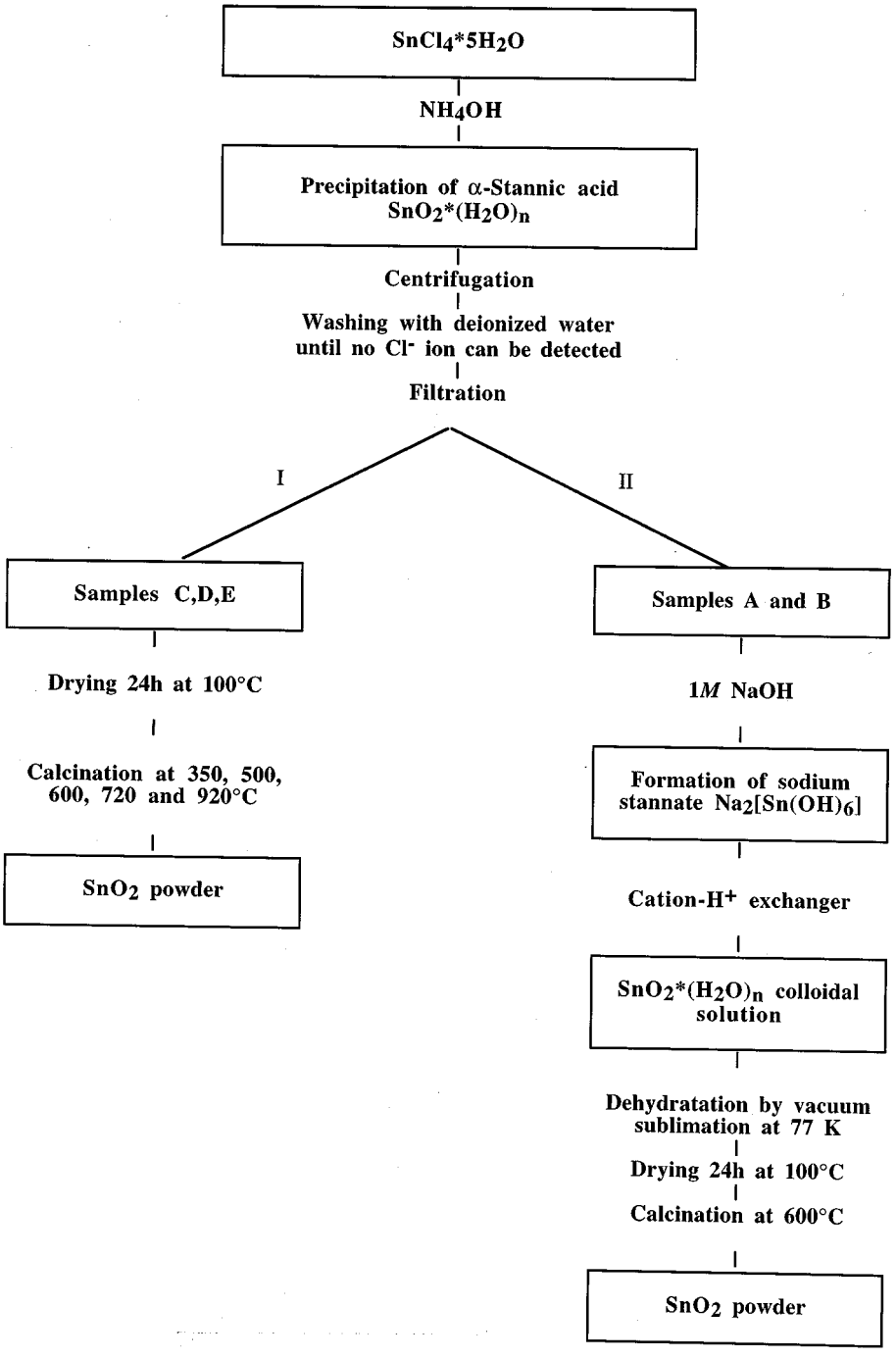

FIG. 1. The two routes followed for preparing nanometric SnO_2 powders: Samples C and D were calcined for 3.5 hr at 720 and 920°C, respectively, sample E was calcined at 600°C for 62 hr and samples A and B were obtained via the colloidal solution step. Sample A was obtained without calcination, and sample B was calcined for 62 hr at 600°C.

one hand and diagrams A and B on the other are indicative of a significant effect of synthesis conditions on the powder microstructures.

The density, size, and shape of the powder particles, observed by SEM, depend on the synthesis process conditions. The powder obtained by route I is made of "two-dimensional" plates (Fig. 4, top) whereas the samples obtained directly from stannic acid via route II consist of "three-dimensional" particles with diameters of 5–7 μm (Fig. 4, bottom).

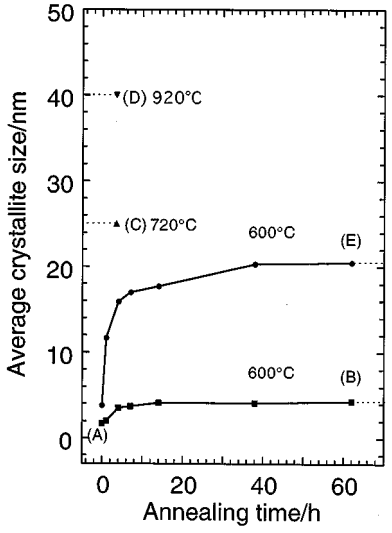

FIG. 2. Conditions of thermal annealing applied to different samples labeled by a capital letter. The average size of the crystallite is deduced from the X-ray diagrams of Fig. 3.

Raman

Figure 5 reports typical spectra for the five powder samples. The spectral range actually investigated was between 100 and 800 cm^{-1}. In contrast to thin films, no particular feature was observed below 400 cm^{-1} and the low-frequency region is not reported in Fig. 5.

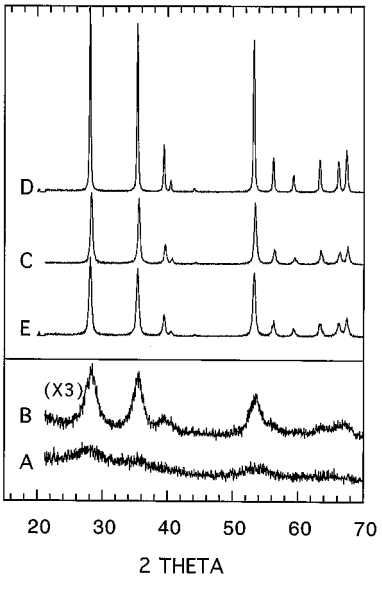

FIG. 3. X-ray diagrams of the different samples studied by Raman spectroscopy: (A) as prepared; (B) annealed at 600°C for 62 hr; (C) annealed at 720°C for 3.5 hr; (D) annealed at 920° for 3.5 hr; (E) annealed at 600° for 62 hr.

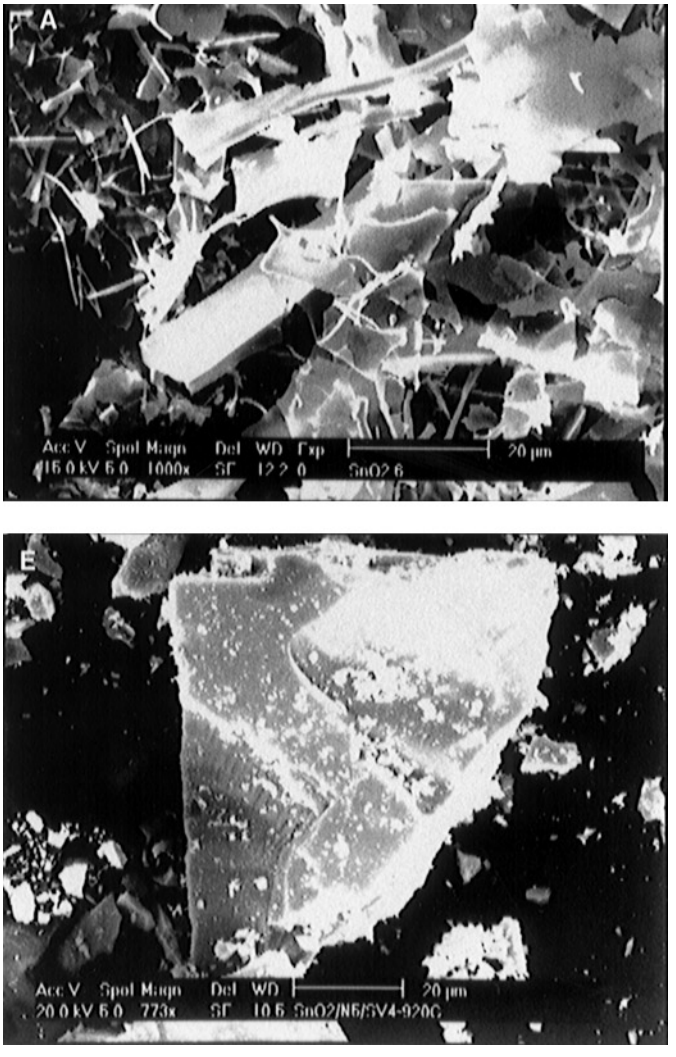

FIG. 4. SEM pictures of samples A and E. Notice the 2D ribbonlike aspect of sample A.

Spectra were fit to Lorentzian functions (also represented in Fig. 5) with Peakfit software from Jandel and each band is characterized by its frequency, amplitude, and half-width. The evolution of these parameters versus the size of crystallites is reported in Table 1. The components representative of volume modes were defined from the single-crystal data of ref 3 and from spectra of a natural cassiterite sample (with a large concentration of defects) and are given in Fig. 5. The additional broad bands whose intensities increase when the size decreases are attributed to the surface modes as suggested in ref 8. The components representative of these modes were identified from the spectrum of sample B and were also tracked in spectra of smaller crystallites (sample A) as well as larger crystallites (sample D). Spectrum B is quite similar to spectra 2 and 3 of ref 8, and spectra C, D, and E are similar to spectrum 6 of ref 8 and that of the 450°C powder represented in Fig. 5 of ref 10. On the contrary, spectrum

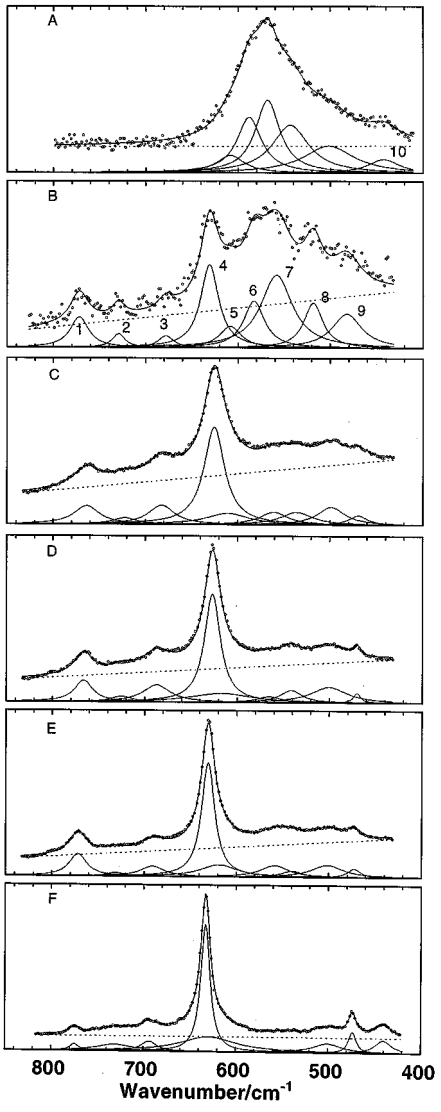

FIG. 5. Raman spectra of samples A–F recorded at 25°C. The continuous line is the result of the fitting procedure.

A is completely different from those reported up to now. It can be considered as representative of very small particles (ca. 2.5 nm) whose aggregation leads to a ribbonlike microstructure (Fig. 4).

The loss of intensity is also a striking observation. Even if the decrease of atomic density is taken into account and if the integrated intensities are considered, one must realize that the intensity loss is related to the reduction of the size of the particles. The lack of continuity of the medium is responsible for strong elastic Rayleigh losses, but the decrease of the Raman cross section with the volume of the scatterer seems to be an intrinsic cause.

The evolution of the spectral parameters (wavenumber, half-width, amplitude) versus the size of the crystallites in spectra A, B, C, D, and F is continuous and is in good agreement with the literature results. High-frequency Raman-active modes, numbered 1–5 in Table 1, decrease with size, while modes at low wavenumbers (modes 6–9) shift to higher wavenumbers. The half-width of mode 4 at about 630 cm^{-1} increases regularly, and the ratio of its integrated intensity to the sum of the intensities of modes 6 and 7 varies as $1/R$.

However, from the crystallite size criterion, spectrum E of the sample annealed for 62 hr at 600°C is expected to be intermediate between spectra B and C. However, it presents a spectrum quite similar to that of the natural SnO_2 crystal (spectrum F). The degree of aggregation could be related to this observation.

Infrared Spectroscopy

The spectra of samples A and B are of particularly high quality (Fig. 6). This likely results from a nanosize effect. These spectra present the same differences as their Raman counterparts. The strong band peaking at 624 cm^{-1} in sample A is actually a shoulder of the main band measured at 564 cm^{-1} in sample B. In the same way, the narrow band at 255 cm^{-1} appearing as a shoulder of the 299-cm^{-1} band in sample B is absent for sample A. The bands which gain intensity from B to A could be associated to volume modes and vice versa. Thus as in the Raman spectra the component at 564 cm^{-1} observed on the low-frequency side of the main IR band is characteristic of the smallest particle size and could be due to surface modes. The most important IR feature is the presence of a strong OH bond stretching centered at 3385 cm^{-1} indicative of the presence of hydroxyl species likely covering the surface of the particles and ensuring the completion of bonds for surface oxygens. Notice that the OH band is stronger for sample A as expected in such a hypothesis.

DISCUSSION

We have defined volume modes as those which derive from crystal normal modes. One can assume that the relaxation of the $k = 0$ selection rule is progressive when the rate of disorder increases or the size decreases. For this reason, one can first track the Raman modes, keeping in mind that IR modes can become weakly active when the structural changes induced by the disorder and the size effects take place. In addition, corner-zone modes, which also coincide with maxima in the density of states (DOS), can also be considered as able to become observable in Raman spectra. Table 1 reports all of these data for the crystals. It is clear from Fig. 5 and Table 1 that volume modes have practically all disappeared in sample A. The spectrum of sample B contains bands of both types.

TABLE 1
Vibrational Spectra of SnO_2 Samples

		Powder						Crystal[a]							
		Raman						Raman	IR	Calculated					
Band	Nature[b]	A	B	C	D	E	F	Γ	Γ	Z	M	Symmetry in Γ	Mode[c] description		
1	V		771.5	763.5	766.5	772	775	782		700		Γ_4^+: B_{2g}	ν_a	SnO	xy
									770		750	Γ_5^+: E_u LO	ν	SnO	xy
2	V		729.5	722.5	725.5	731	731.5								
3	V		678	686.5	687	691	694		705	700		Γ_1^-: A_{2u} LO	ν	SnO	z
4	V	607	631	625.5	627	630.5	632.5	638		550		Γ_1^+: A_{1g}	ν_s	SnO	xy
5	V		608	611	617	619	630		618			Γ_5^+: E_u TO	ν	SnO	xy
6	S	589	582.5	561	565.5	558.5									
7	S	567	558	536	541.5	539.5				550		Γ_4^-: B_{1u}	δ	SnOSn	z
8	V	540	518.5	498.5	500.5	501.5	498		477		470	Γ_1^-: A_{2u} TO	ν	SnO	z
9	S	502	482								500	Γ_4^-: B_{1u}	δ	SnOSn	z
10	V	443		469.5	470	472.5	473	476		500		Γ_5^-: E_g	T′	O	z
							420								
									366						
									290						
									226						
	D (nm)[d]	2.5	4.5	25	40	20	> 100	> 100							
	$\Gamma(4)$ (cm^{-1})[e]	18	15	14	10	8.3	6	1							
	$A(4)$[f]	132	594	6428	5457	9616									
	$A(6)$[f]	419	338	834	292	968									
	I_4/I_{6+7}[g]	0.15	0.46	2.6	4.2	3.2									
	N_S/N_V[h]	0.32	0.18	0.032	0.02	0.04	< 0.001								

Note. Samples A and B were prepared following route II; samples C, D, and E were prepared following route I.
[a] The Raman, IR, and neutron or calculated data are from refs. 3–5, respectively.
[b] V is for volume mode, and S is for surface mode.
[c] The description of the modes is deduced from ref 11. ν is for bond stretching, δ is for bond bending, and T is for translation as a whole (acoustic modes).
[d] Diameter (nm) of crystallites deduced from X-ray diagrams of Fig. 3 for the different samples.
[e] Half-width (cm^{-1}) of mode 4 for the different samples.
[f] Amplitude of mode 4 in the different samples.
[g] Ratio of the integrated intensities of volume mode 4 and of surface modes 6 and 7.
[h] Ratio of surface to volume atoms versus the dimensions of crystallites. $N_S/N_V = [4(D/2)^2/r^2][r^3/(\frac{1}{2}D)^3] = 8r/D = 0.8/D$ nm.

Volume Modes

As already stated, no clear Raman bands are observed below 400 cm^{-1} in either the crystal or the powder spectra. Note that the modes giving rise to one-phonon DOS (Fig. 7 in ref 5) below 400 cm^{-1} are not Raman induced by disorder. However, weak Raman bands 3 and 8, which are measured at 694 and 498 cm^{-1}, respectively from sample F to sample B, seem to correspond to IR-active LO and TO A_{2u} modes. For sample B these modes are separated by 160 cm^{-1}, while in the crystal the TO–LO splitting is 230 cm^{-1}. Thus it seems reasonable to assign these volume modes to IR modes whose Raman activity is induced by disorder. The TO–LO splitting decrease is a direct consequence of the crystallite size decrease. Bands 2 and 5 are extremely weak; they are still present in sample B, but both have disappeared in sample A. (The component reported at 607 cm^{-1} is rather a rest of mode 4 strongly downshifted rather than the above mode 5). These modes could correspond to the LO–TO E_u IR-active modes.

The frequency of the volume modes 1, 4, and 10 systematically decreases with the size. This can be interpreted on the basis of a tensile state which should develop progressively in the bulk of crystallites when their surface contribution increases. This statement implies a concept of mechanical balance between volume stresses and surface tensile stresses.

Surface Modes

Spectrum 5A is particularly representative of the surface vibrational dynamics. Modes 6 and 7 (Table 1) can be easily tracked in samples A and B. It is also possible to identify weak bands in samples D and E. The evolution of the relative intensity of these modes can be represented through the ratio of the sum of the integrated intensities of modes 6 and 7 to the integrated intensity of the volume mode 4.

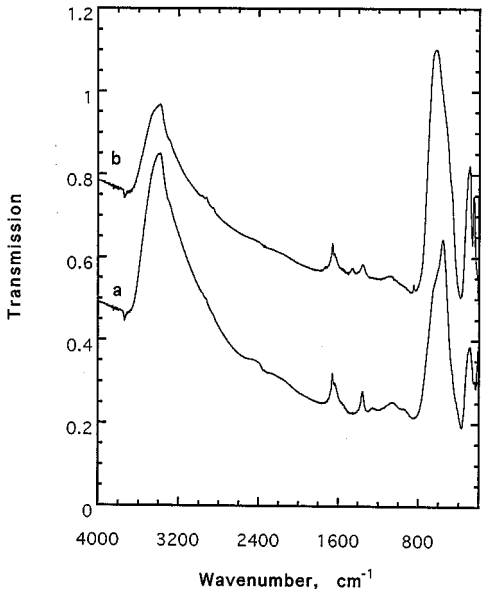

FIG. 6. Infrared spectra of samples A (a) and B (b) recorded at 25°C. The measured wavenumbers are (a) 3500 (broad), 3386, 630 (shoulder), 564, and 292 cm^{-1} and (b) 3500, 3384, 624, 299, and 255 cm^{-1}.

This ratio varies as the reciprocal of the size of the crystallites in the 2- to 40-nm range. This trend is similar to that of Fig. 2 of ref 8, which represents the amplitude ratio of the same bands. However, we would like to make two comments on this work: (i) We think that the integrated intensity parameter is preferable to the amplitude one. (ii) Zuo *et al.* (8) considered the ratio of the number of surface atoms N_S to the total number of atoms and plotted this quantity versus the crystal size (Fig. 3 in ref 8). Assuming that the particles are spherical, we do not find the same values for an average ionic radius of 0.1 nm and a particle radius of 5 nm (i.e., a crystal size of 10 nm). We find $N_S/N_T = 0.15$ instead of 0.25 as in the work of Zuo *et al.* Moreover, the ratio N_S/N_V, with N_V the number of volume atoms, is more representative of the intensity variations, at least for the crystallite sizes investigated currently. To explore the shape effect on this ratio, we have considered two situations of platelet-like particles: one has thin particles able to correspond to sample A, with $D_z = 2$ nm and in plane dimensions varying from $D_x = 100$, $D_y = 100$ (giving $N_S/N_V = 0.2$) to $D_x = 2$, $D_y = 2$ (giving $N_S/N_V \gg 1$) (in that case, $N_S/N_T = 1$). The other situation is described by $D_z = 20$ nm with large dimensions in the x and y directions and leads to $N_S/N_V = 0.02$. This situation could correspond to sample E for which there is a systematic discrepancy between spectral parameters expected from size considerations and those which are observed.

The general frequency trend is to decrease when the crystallite size increases; i.e., it is the reverse trend of the volume modes. In terms of surface structural change, one can consider that surface tensile stresses decrease as the lattice energy of surface atoms becomes less and less imposed by the volume atoms but results in the renormalization of their organization.

One can now try to describe the normal modes associated with these bands:

Modes 7 and 9, identified as surface modes, fall in the same frequency range as the Γ_4^- modes of the crystal in the Z and M points of the Brillouin zone. These modes involve z displacements of atoms (Fig. 3 in ref 11) and correspond to bending coordinates. They are inactive in Raman and IR and it is unlikely that they could give rise to the relatively strong Raman band at about 550 cm^{-1}. We prefer to keep the intensity criterion which consists of associating a strong Raman band to a symmetric mode and in the present case to a stretching of the SnO bonds in the octahedra similar to the volume mode 4 at about 630 cm^{-1}; its wavenumber should be downshifted by the fact that some oxygen atoms are not bonded to neighboring Sn atoms and thus bonds are weakened.

CONCLUSIONS

Tin dioxide nanocrystalline powders were prepared by two routes. Those obtained via a colloidal solution step led to nanometric (2.5 nm) particles giving aggregates having a particular two-dimensional microstructure. Raman spectra of these compounds are original compared to those reported in the literature.

As reported in the literature, the Raman spectral signature was found to change drastically with the size of the particles. Contrary to literature studies, which report a broadening of spectra with the decrease of the size of crystallites and interpret these observations with models such as that of phonon confinement, we have not observed a dramatic broadening of the usual crystal modes. Instead, as stated in recent papers, new bands were found to grow with the proportion of surface atoms. The spectra of these new nanometric compounds allowed us to identify specific surface modes and a continuous assignment of the volume and surface modes for different tin dioxide powders is presented. Their frequency evolution with crystallite size is discussed in terms of surface stresses.

ACKNOWLEDGMENTS

O. Chaix and M. Boulova are acknowledged for their contribution in obtaining the IR measurements.

REFERENCES

1. K. L. Chopra, S. Major, and D. K. Pandya, *Thin Solid Films* **102,** 1 (1993).
2. D. Kohl, *Sens. Actuators, B* **1,** 158 (1990).

3. R. S. Katiyar, P. Dawson, M. M. Hargreave, and G. R. Wilkinson, *J. Phys. C*: *Solid State Phys.* **4,** 2421–2431 (1971).
4. F. Gervais and W. Kress, *Phys. Rev. B* **31,** 4809 (1985).
5. T. Sato and T. Asari, *Phys. J. Soc. Jpn.* **64** (4), 1193–1199 (1995).
6. J. T. Luxon and R. Summitt, *J. Chem. Phys.* **50** (3), 1366–1370 (1969).
7. M. Ocana and C. J. Serna, *Spectrochim. Acta*, *Part A*, **47** (6), 765–774 (1991).
8. J. Zuo, C. Xu, X. Liu, C. Wang, Y. Hu, and Y. Chian, *J. Appl. Phys.* **75** (3), 1835–1836 (1994).
9. C. Xie, L. Zhang and C. Mo, *Phys. Status Solidi. A* **141,** K59–61 (1994).
10. A. Dieguez, A. Romano-Rodriguez, J. R. Morante, U. Weimar,M. Schweizer-Berberich, and W. Gőpel, *Sens. Actuators*, *B* **31,** 1–8 (1996).
11. J. G. Traylor, H. G. Smith, R. M. Nicklow, and M. K. Wilkinson, *Phys. Rev. B* **3,** 3457–3471 (1971).
12. C. Pigenet and F. Fievet, *Phys. Rev. B* **22,** 2785–2791 (1980).
13. H. Richter, Z. P. Wang, and L. Ley, *Solid State Commun.* **39,** 625–629 (1981).
14. I. Campbell and P. Fauchet, *Solid State Commun.* **58,** 739 (1986).
15. E. Roca, C. Trallero-Giner, and M. Cardona, *Phys. Rev. B* **49,** 13704 (1994).
16. L. Saviot, B. Champagnon, E. Duval, I. Kudriatsev, and A. Ekimov, *J. Non-Cryst. Solids* **197,** 238 (1996).